View metadata, citation and similar papers at core.ac.uk
brought to you by CORE
provided by DSpace@MIT

PSFC/JA-98-10

Experimental and Theoretical Investigations of a 17 GHz RF Gun

W. J. Brown, S. Trotz* , K. E. Kreischer, M. Pedrozzi,
M. A. Shapiro, R. J. Temkin

April 1998

Plasma Science and Fusion Center
Massachusetts Institute of Technology
Cambridge, MA 02139 USA

**Present Address: Dartmouth College, Hanover, NH*

This work is supported by the U.S. Department of Energy under contract number DE-FG02-91ER40648.

Submitted for publication to *Nuclear Instruments and Methods in Physics Research A.*

ABSTRACT

We report on experimental and theoretical investigations of a 17 GHz RF photocathode electron gun. This is the first photocathode electron gun to operate at a frequency above 2.856 GHz. The 1.5 cell, π–mode, copper cavity was tested with 50 ns pulses from a 17.150 GHz klystron amplifier built by Haimson Research Corp. A Bragg filter was used at the RF gun to reduce the reflection of parasitic modes back into the klystron. Coupling hole theory in conjunction with cold test measurements was used to determine the field profile in the RF gun. The particle in cell code MAGIC as well as coupled envelope equations were used to simulate the beam dynamics in the RF gun. With power levels of 4 MW, the on axis electric field at the cathode exceeds 300 MV/m, corresponding to an average accelerating gradient of 200 MV/m over the first half cell of the gun. Breakdown was observed at power levels above 5 MW. Electron bunches were produced by 20 μJ, 1 ps UV laser pulses impinging on the RF gun copper photocathode and were measured with a Faraday cup to have up to 0.1 nC of charge. This corresponds to a peak current of about 100 A, and a density at the cathode of 8.8 kA/cm^2. Multiple output electron bunches were obtained for multiple laser pulses incident on the cathode. Phase scans of laser induced electron emission reveal an overall phase stability of better than ±20°, corresponding to ±3 ps synchronization of the laser pulses to the phase of the microwave field. A Browne-Buechner magnetic spectrometer indicated that the RF gun generated 1 MeV electrons with a single shot rms energy spread of less than 2.5%, in good agreement with theoretical predictions.

1 INTRODUCTION

The goal of the 17 GHz photocathode RF gun experiment is to construct an ultra high brightness source of electrons which can be used for future linear colliders or free electron lasers and to demonstrate the practicality of high gradient (several hundred MV/m) acceleration. The photocathode RF gun is a novel electron beam source intended to meet the requirements set by future high-energy linear colliders and next generation free electron lasers. A coupled pair of pillbox TM_{010}-like resonators is excited by sidewall coupled microwaves at 17.15 GHz (Fig. 1). Note that the axial length of the structure is determined by the microwave wavelength. A picosecond ultraviolet laser pulse illuminates the back wall of the structure at the axis of symmetry. Electrons are released by the photoelectric effect and are accelerated by the axial electric field.

Initial operation of the MIT 17.15 GHz RF gun was reported in 1996 [1]. Previous photocathode RF gun experiments have operated at 3 GHz or below [2-10], though an RF gun experiment at 8.5 GHz is currently under development [11]. There has also been much theoretical work in the study of RF guns in recent years [12-17]. From an analysis of the Vlasov-Maxwell equations governing the dynamics of the electron beam production in the photocathode RF gun, the scaling with RF frequency of the quality of the beam which can be produced in an RF gun has been derived [15,16]. One of the major advantages of going to higher frequency is that the emittance of the beam increases linearly with RF frequency, implying a quadratic increase in the beam brightness. The implication of this is that high frequency RF guns are very promising candidates for use with future high energy electron colliders and short wavelength free electron lasers, both of which will require extremely high brightness beams beyond the capabilities of more conventional electron sources. In this experiment, we have measured the bunch charge and energy of the beam produced from the 17 GHz RF gun, demonstrating successful operation of the RF gun and its robustness to repeated exposure to ultra high gradient electric fields and significant temperature rises due to power dissipation.

2 THEORY AND DESIGN

The two modes of a 1 ½ cell structure like the MIT RF Gun are illustrated in Fig. 2. These were obtained from SUPERFISH [18] simulations for a cavity design slightly perturbed from the actual RF Gun dimensions. The two cells can be modeled as coupled TM_{010} oscillators which have corresponding symmetric and anti-symmetric oscillations. For acceleration purposes, the mode in which the two cavities oscillate 180 degrees out of phase with one another, the π-mode, is the preferred mode of excitation. Then, provided the full cell length L is equal to one half of the vacuum wavelength λ of the accelerating microwaves, relativistic electrons will remain in phase with the RF fields in the cavity. In order to obtain equal field magnitudes in both the half and full cell, the frequency separation of the 0 and π modes should be near a minimum (albeit, not exactly at the minimum), in accordance with elementary coupled harmonic oscillator theory. The radius of each cell, on which the resonant frequencies are primarily dependent, is therefore a critical design parameter. If the relative dimensions of the two cells are slightly off optimum, resulting in a large mode separation, the 0 and π modes become essentially the separate resonances of each cell with a correspondingly unbalanced field profile.

2.1 Effects of Coupling

In actuality, consideration of the half and full cell dimensions is not sufficient to produce a balanced RF gun. The mechanism for coupling power into the gun can produce a significant perturbation of both the mode separation as well as the inter-cavity coupling, resulting in π and 0 mode profiles which are drastically different from the unperturbed case. We present a theory to account for such effects in determining the actual field profile of the excited mode in the RF Gun, which we express as a linear combination of the unperturbed 0 and π mode profiles obtained from SUPERFISH simulations.

The MIT RF Gun is excited via coupling holes placed an integer number of guide quarter wavelengths, $\lambda_g = 2\pi/k_{gz}$, from the reflecting short of a WR-62 waveguide (Fig. 1). The waveguide is excited in the fundamental TE_{10} mode, which leads to $k_{gz} = \sqrt{\frac{\omega^2}{c^2} - \frac{\pi^2}{a^2}}$ where a is the broad wall dimension of the waveguide. The reflecting short induces a standing wave field pattern such that an axial z-component of magnetic field given by

$$H_{gz} = -i\frac{\pi c}{\omega a}\frac{E_{10}}{Z_0}\cos\left(\frac{\pi x}{a}\right) \qquad (1)$$

exists at the broad wall of the waveguide at the z position of the coupling holes, where E_{10} is the electric field amplitude of the TE_{10} mode in the waveguide and $Z_0 = \sqrt{\frac{\mu_0}{\varepsilon_0}} =$ 377 Ohms. This magnetic field is parallel to the azimuthal component of the magnetic field of the TM_{01} (0 or π mode) in the cavity. The coupling holes are cut along these magnetic field components resulting in magnetic coupling. Following coupling hole theory [19], this allows the coupling to be represented as magnetic dipoles *m(1)* and *m(2)* oriented along the long axis of the coupling holes in the half and full cell respectively. The magnetic dipole moment m is proportional to the total magnetic field at the hole (from both cavity side and waveguide side), $m = \alpha H$, where α is the polarizability of the hole.

Using the theory of cavity excitation [19], we describe the actual mode excited in the RF gun by the magnetic dipoles *m(1)* and *m(2)* in terms of complex amplitudes of the 0 and π modes of the unperturbed RF gun (i.e. without coupling holes). These relative amplitudes depend on the polarizabilities of both coupling holes (α_1 and α_2), the dimensions a and b of the waveguide, and the ratio of the square of the magnetic field at each coupling hole to the stored energy in the cavity for both the 0 and π modes. These last four quantities can be obtained from SUPERFISH simulations and will be denoted by

$\frac{H_{S0}^2(1)}{W_{S0}}$, $\frac{H_{S0}^2(2)}{W_{S0}}$, $\frac{H_{Sp}^2(1)}{W_{Sp}}$, and $\frac{H_{Sp}^2(2)}{W_{Sp}}$, where $H_{S0}(1)$, $H_{S0}(2)$, $H_{Sp}(1)$, and $H_{Sp}(2)$ are the SUPERFISH values of the magnetic field of the unperturbed 0 and π modes at the location of coupling holes 1 and 2 respectively, while W_{S0} and W_{Sp} are the corresponding stored energies of the unperturbed 0 and π modes. The complex amplitudes of these two modes are given by

$$A_{S0} = -2\frac{i\mathsf{p}\mathsf{e}_0 Z_0 \mathsf{w}^2(\tilde{m}(1)H_{S0}(1) + \tilde{m}(2)H_{S0}(2))}{(\mathsf{w}^2 - \mathsf{w}_{S0}^2)W_{S0}} \tag{2}$$

and

$$A_{Sp} = -2\frac{i\mathsf{p}\mathsf{e}_0 Z_0 \mathsf{w}^2(\tilde{m}(1)H_{Sp}(1) + \tilde{m}(2)H_{Sp}(2))}{(\mathsf{w}^2 - \mathsf{w}_{Sp}^2)W_{Sp}}, \tag{3}$$

where $\tilde{m} \equiv m\frac{Z_0}{E_{10}}$ is a normalized magnetic moment with units of polarizability, $\omega = 2\pi f$ is the operating circular frequency (i.e. the klystron frequency), and

$$\mathsf{w}_{S0} = 2\mathsf{p}f_{S0}\left(1 - \frac{i}{2Q_{S0}}\right) \tag{4}$$

and

$$\mathsf{w}_{Sp} = 2\mathsf{p}f_{Sp}\left(1 - \frac{i}{2Q_{Sp}}\right) \tag{5}$$

are the SUPERFISH 0 and π mode complex frequencies where Q_{S0} and Q_{Sp} are the quality factors of the unperturbed 0 and π modes calculated from SUPERFISH. For a given drive frequency, w, the actual mode excited in the RF gun can now be expressed in terms of the SUPERFISH 0 and π modes and their corresponding complex excitation

amplitudes. For example, the actual on axis longitudinal electric field profile in the RF gun is given by

$$\tilde{E}_z(z,\omega) = A_{S\pi}(\omega)E_{S\pi z}(z) + A_{S0}(\omega)E_{S0z}(z) \ , \tag{6}$$

where $E_{S\pi z}(z)$ and $E_{S0z}(z)$ are the SUPERFISH on axis longitudinal electric fields for the unperturbed π and 0 modes respectively and $\tilde{E}_z \equiv \frac{E_z}{E_{10}}$ is the actual field profile normalized to the magnitude of the waveguide electric field. Note that the choice that the z direction coincide with the RF gun symmetry axis differs from the waveguide coordinate system shown in Fig. 1.

Using the theory of waveguide excitation [19], we also calculate the complex reflection coefficient, S_{11}, of the TE_{10} mode in the WR-62 waveguide from the RF gun to be

$$S_{11} = -1 + \frac{4\pi^2\omega}{ca^2bk_{gz}}\left(\tilde{m}(1)\cos\frac{\pi x_1}{a} + \tilde{m}(2)\cos\frac{\pi x_2}{a}\right), \tag{7}$$

where x_1 and x_2 are the positions of the coupling holes along the broad wall of the waveguide and c is speed of light.

The expressions for the magnetic moments $\tilde{m}(1)$ and $\tilde{m}(2)$ can be determined self-consistently using the cavity and waveguide excitation formulas (2), (3) and (7) to obtain

$$\tilde{m}(1) = i\frac{c}{\omega a}\frac{-\alpha_1\Lambda_{22}\cos\frac{\pi x_1}{a} + \alpha_2\Lambda_{12}\cos\frac{\pi x_2}{a}}{\Lambda_{11}\Lambda_{22} - \Lambda_{12}\Lambda_{21}} \tag{8}$$

and

$$\tilde{m}(2) = i\frac{c}{\omega a}\frac{\alpha_1\Lambda_{21}\cos\frac{\pi x_1}{a} - \alpha_2\Lambda_{11}\cos\frac{\pi x_2}{a}}{\Lambda_{11}\Lambda_{22} - \Lambda_{12}\Lambda_{21}} \quad , \tag{9}$$

where

$$\Lambda_{11} = 1 + \frac{2\pi\varepsilon_0 Z_0^2\omega^2\alpha_1 H_{S0}^2(1)}{(\omega^2 - \omega_{S0}^2)W_{S0}} + \frac{2\pi\varepsilon_0 Z_0^2\omega^2\alpha_1 H_{Sp}^2(1)}{(\omega^2 - \omega_{Sp}^2)W_{Sp}} - \frac{4i\pi^3\alpha_1\cos^2\frac{\pi x_1}{a}}{a^3 b k_{gz}},$$

$$\Lambda_{12} = \frac{2\pi\varepsilon_0 Z_0^2\omega^2\alpha_1 H_{S0}(1)H_{S0}(2)}{(\omega^2 - \omega_{S0}^2)W_{S0}} + \frac{2\pi\varepsilon_0 Z_0^2\omega^2\alpha_1 H_{Sp}(1)H_{Sp}(2)}{(\omega^2 - \omega_{Sp}^2)W_{Sp}} - \frac{4i\pi^3\alpha_1\cos\frac{\pi x_1}{a}\cos\frac{\pi x_2}{a}}{a^3 b k_{gz}},$$

$$\Lambda_{21} = \frac{2\pi\varepsilon_0 Z_0^2\omega^2\alpha_2 H_{S0}(1)H_{S0}(2)}{(\omega^2 - \omega_{S0}^2)W_{S0}} + \frac{2\pi\varepsilon_0 Z_0^2\omega^2\alpha_2 H_{Sp}(1)H_{Sp}(2)}{(\omega^2 - \omega_{Sp}^2)W_{Sp}} - \frac{4i\pi^3\alpha_2\cos\frac{\pi x_1}{a}\cos\frac{\pi x_2}{a}}{a^3 b k_{gz}},$$

and

$$\Lambda_{22} = 1 + \frac{2\pi\varepsilon_0 Z_0^2\omega^2\alpha_2 H_{S0}^2(2)}{(\omega^2 - \omega_{S0}^2)W_{S0}} + \frac{2\pi\varepsilon_0 Z_0^2\omega^2\alpha_2 H_{Sp}^2(2)}{(\omega^2 - \omega_{Sp}^2)W_{Sp}} - \frac{4i\pi^3\alpha_2\cos^2\frac{\pi x_2}{a}}{a^3 b k_{gz}}.$$

The energy conservation law is expressed as

$$|S_{11}|^2 + \frac{2\pi f_{S0}|A_{S0}|^2\left(\omega^2 + |\omega_{S0}|^2\right)W_{S0}}{Q_{S0}\omega\varepsilon_0 c^2 abk_{gz}} + \frac{2\pi f_{Sp}|A_{Sp}|^2\left(\omega^2 + |\omega_{Sp}|^2\right)W_{Sp}}{Q_{Sp}\omega\varepsilon_0 c^2 abk_{gz}} = 1 \ . \tag{10}$$

Thus far, we have described a theory that completely describes the cavity filling and mode mixing characteristics of the RF gun provided the polarizabilities of the coupling holes are known. For holes of simple geometry, these polarizabilities can be calculated

analytically. Particularly, for an elliptical hole whose dimensions are major radius $\frac{dz}{2}$ and minor radius $\frac{dx}{2}$ (Fig. 3), the polarizability is $\alpha = \frac{\pi (dz/2)^3 e^2}{3[K(e) - E(e)]} f(t)$ in SI units. Here $e = \sqrt{1-(dz/dx)^2}$, $K(e)$ and $E(e)$ are elliptical integrals, and the function $f(t)$ of coupling wall thickness t can be determined using advanced theory [20] ($f(0) = 1$ for infinitely small thickness). For the case of the RF gun dimensions, we can make an elliptical approximation with $dz_1 = dz_2 = 0.508$ *cm*, $dx_1 = 0.165$ *cm*, $dx_2 = 0.229$ *cm* and an average wall thickness t=0.025 cm. According to theory [20], the factor $f(t)$ ranged from 0.49 to 0.52 for such coupling hole dimensions. As a result, the directly calculated polarizabilities are $\alpha_1 = 5.28 * 10^{-9} m^3$ and $\alpha_2 = 6.62 * 10^{-9} m^3$.

Fig. 4 shows the S_{11} frequency dependence calculated using these values compared with an experimentally determined S_{11} curve. It is seen that the elliptical approximation used to describe the coupling holes is only approximate and can not be used to accurately describe the cavity coupling characteristics. Determination of the actual polarizabilities of the coupling holes is complicated by the non-elliptical shape of the holes as well as the non-uniform thickness across the holes. In order to obtain accurate results, the polarizabilities α_1 and α_2 of the holes need to be considered as free parameters of the coupling theory described above. These parameters can then be determined from comparison of an S_{11} curve obtained from experimental cold tests of the cavity and the theoretically calculated S_{11} curves given by equation (7).

2.2 Characteristics of the Actual Cavity

In order to completely characterize the filling characteristics of the RF gun, certain critical parameters must be experimentally determined. The most important of these parameters are the coupling coefficient β_c of the cavity and its ohmic quality factor, Q_{cav}. These two quantities dictate the attainable stored energy in the RF gun for a given

incident power, P_{inc}. As described in the previous section, this stored energy can be expressed as a mixture of the two unperturbed (i.e. no coupling holes) modes calculated by SUPERFISH. Accurate determination of the relative amplitude of excitation of these two modes requires an experimental measurement of the polarizabilities, α_1 and α_2, of the coupling holes. These four parameters (β_c, Q_{cav}, α_1, and α_2) along with the knowledge of the field profiles of the unperturbed *0* and π modes completely characterize the RF gun.

In order to obtain values for the Q, β_c, and polarizabilities of the RF gun (Table 1), cold tests of the cavity were performed using an HP 8510 Vector Network Analyzer. These tests consisted of the measurement of both the amplitude and phase of the reflection coefficient of the power incident on the RF gun, $|S_{11}| = \sqrt{\frac{P_{refl}}{P_{inc}}}$, where P_{refl} is the total reflected power. The coupling coefficient is defined to be the ratio of the cavity quality factor to the external quality factor ($\beta_c = Q_{cav}/Q_{ext}$) and can be determined from the measurement of $|S_{11}|$ at resonance from the expression

$$|S_{11}|_{resonance} = \left|\frac{1-\beta_c}{1+\beta_c}\right| . \qquad (11)$$

For our cavity, $S_{11} = 0.22$ at the resonant frequency of 17.142 GHz, which gives a coupling coefficient of $\beta_c = \frac{1+|S_{11}|}{1-|S_{11}|} = 1.56$ for an overcoupled cavity while Q_L is determined from the width of the resonance at the level of $|S_{11}| = \frac{\sqrt{1+\beta_c^2}}{1+\beta_c} = 0.72$ and is equal to 1060. The unloaded quality factor is then given by $Q_{cav} = Q_L(1+\beta_c) = 2700$. The power dissipated in the cavity, P_{cav}, is determined by the coupling coefficient β_c:

$$P_{cav} = \frac{4\beta_c}{(1+\beta_c)^2} P_{inc} = 0.95 P_{inc} \ . \qquad (12)$$

Expressions (11) and (12) are only valid assuming a single mode. Note that while the excited mode is being expressed as a combination of the two SUPERFISH modes, it is nevertheless a pure mode of the actual RF Gun/coupling hole system, thus the single mode expressions are valid. As shown below, the great majority of the stored energy at this resonance is in the unperturbed π mode, thus the measured quality factor of the cavity should be similar to the SUPERFISH Q_{Sp}. The measured Q_{cav}=2700 for the π mode in the experimental cavity is 70% of the calculated SUPERFISH value.

The actual polarizabilities of the coupling holes are determined by matching equation (7) to the measured S_{11} curve. Specifically, the polarizabilities α_1 and α_2 are determined to match the measured resonances at 17.142 and 17.118 GHz (Fig. 4). This leads to the values of the polarizabilities listed in Table 1. The resulting ratio of the amplitudes of excitation of the 0 and π modes is $A_{S0}/A_{Sp} = (0.815 - i4.648)/(-0.227 + i12.817)$ for 17.142 GHz. The field profile in the RF gun can now be determined using equation (6) along with the known field profiles of the unperturbed 0 and π modes, which are shown in Fig. 5. The resulting superposition of modes is plotted in Fig. 6. The ratio of energy stored in the unperturbed π mode to that in the unperturbed 0 mode is about equal to 20 for the operating frequency of 17.142 GHz. Note that the field strength in the first cell is almost 5 time larger than the field strength in the second cell. While this is not ideal for efficient acceleration, it does facilitate the production of ultra high gradients in the first cell by lowering the incident power required to reach a given electric field at the cathode.

It should also be noted that the current RF gun geometry and resulting cold test results mentioned here differ from those of the originally constructed RF gun in that the full cell diameter was increased by about 0.13 mm (about 0.9 %) after initial cold testing revealed a large mode separation and a π mode almost entirely in the full cell alone. Increasing the full cell radius significantly improved the field balance of the RF gun and brought the π mode resonant frequency closer to the ideal operating frequency of the klystron.

2.3 Effects of a Partially Reflecting Short

In the experimental determination of the cavity coupling characteristics described above, a perfectly reflecting short at the end of the waveguide was used. However, in the high power experiments, the short was replaced with a Bragg filter (see section 4**)** to eliminate the reflection of spurious higher frequency modes produced by the klystron. At the RF gun resonant frequency of 17.142 GHz, the reflection coefficient, *R*, of the Bragg filter was found to be about 0.67 rather than the ideal value of unity. In order to account for effects of the partially transmitted wave in the coupling theory, we modify the single-mode RF filling expressions to account for a reflection coefficient *R* not equal to 1. For *R* = 0.67 and coupling coefficient β_c = 1.56, the expressions for S_{11} at resonance, the cavity dissipated power P_{cav}, and the external quality factor Q_{ext} are given by

$$S_{11}(\omega_{res}) = \left| \frac{R - \frac{1+R}{2}\beta_c}{1 + \frac{1+R}{2}\beta_c} \right| = 0.27 \quad , \tag{13}$$

$$P_{cav} = \frac{(1+R)^2 \beta_c}{(1 + \frac{1+R}{2}\beta_c)^2} P_{inc} = 0.82 P_{inc} \quad , \tag{14}$$

and

$$Q_{ext} = \frac{2}{1+R}\frac{Q_{cav}}{\beta_c} = 2070 \quad . \tag{15}$$

We can use these expressions to estimate the maximum electric field at the cathode assuming a steady state. Using the measured value for Q_{cav} (Table 1), equation (14), and SUPERFISH simulation results for the electric field magnitude and stored energy we wind up with a steady state expression for the cathode electric given by

$$E_{cathode}[MV/m] = 183\sqrt{P_{inc}[MW]} \quad , \tag{16}$$

which gives $E_{cathode}$ = 366 MV/m for an incident power of 4 MW. In the experiments, however, $E_{cathode}$ is obtained as a function of time through integration.

The "two-mode" coupling theory formulated in section 2.1 has also been modified to account for the Bragg filter. Theoretical and measured S_{11} curves are plotted in Fig. 7. In the future, the Bragg filter will be modified to achieve a reflectivity close to unity.

2.4 Simulations of Beam Dynamics

Extensive simulations of the beam dynamics in the MIT 17 GHz RF Gun have been performed. The expected beam parameters include an initial bunch length of 0.3 mm (1 ps) and a total space charge of 0.1 nC. Results of single particle 1-D simulations as well as 2-D simulations (2-D in fields, 3-D in particle motion) using MAGIC [21] were employed to examine the single particle (i.e. low space charge) dynamics. The effects of space charge were examined by use of coupled envelope equations as well as MAGIC simulations.

The 1-D model employed is a simple integration of the equation of motion,

$$\frac{1}{m}\frac{dp}{dt} = c\gamma^3\frac{d\beta}{dt} = \frac{e}{m}\left(E_i(z)\sin(\omega t) + E_r(z)\cos(\omega t)\right) \quad , \tag{17}$$

where $E_i(z)$ and $E_r(z)$ are the RF gun on axis electric field profiles given in Fig. 6, $\beta = v/c$, and $\gamma = \left(1-\beta^2\right)^{-1/2}$. The space and time dependence of the electric field can also be expressed in the form $E(z,t) = |E(z)|\sin(\omega t + \varphi)$, where φ is an approximately constant function of z except for an 180 degree phase shift between the first and second cells. It is shown (Fig. 8) that 1 MeV electrons are to be expected given a maximum field gradient

at the cathode of about 300 MV/m. Defining the phase $\varphi \equiv \omega t + \theta(z=0)$, it is also seen from the single particle simulation that there are optimum phases of injection for minimization of energy spread and maximization of beam bunching. Bunching corresponds to a negative slope of transit time vs. injection phase, and generally occurs for injection phases < 45 degrees. The 2-D MAGIC simulations with very low space charge (Fig. 9) show good agreement with the 1-D single particle simulations.

The effects of space charge on the beam dynamics can be seen from the MAGIC simulations shown in Fig. 9. Perhaps the most notable effect is the increase in energy spread of the beam. Also, there is no longer any minimum in energy spread or emittance, as they are both seen to monotonically increase with increasing injection phase. The reason for this behavior is that for space charge dominated beams, the RF effects which determine the single particle dynamics are no longer the dominant factor in the transverse dynamics of the beam propagation. For this case of high space charge, the simulations suggest that for low injection phases (φ < *30* degrees), we should expect to produce a beam with a rms energy spread of about 1.5% and an rms geometric emittance of about 0.1 mm-mrad (0.3 mm-mrad normalized). This corresponds to a brightness, *B,* of about 1000 A/(πmm-mrad)^2, where brightness is expressed as

$$B = \frac{I}{\varepsilon_{xn}\varepsilon_{yn}}, \tag{18}$$

where I is the peak current of the beam and ε_n is the normalized transverse rms emittance.

The effects of space charge on the beam dynamics can be analytically examined with the method of coupled envelope equations [22]. We use the axial motion equation and two envelope equations for bunch envelope dimensions. The motion equations for the relativistic factor γ and the electron phase, $\Phi = \omega t - k_z z$, are given by

$$\gamma' = 2a_{acc} k_z F(z) \sin(\Phi + k_z z) \tag{19}$$

and

$$\Phi' = k_z(1/\beta - 1) \ , \tag{20}$$

where the prime denotes a derivative on z , $k_z = \omega / c$ is the axial wavenumber, $\alpha_{acc} = \frac{eE_{cathode}}{2mc^2 k_z}$ is the accelerating parameter at the cathode, and *F(z)* is the normalized field distribution in the RF gun. Note that equation (19) is simply a transformed version of (17) with *F(z)* incorporating the combined profile of the real and imaginary fields. Also note that κ is not the same as the η defined earlier.

The equations for the bunch radius r_m and bunch length $2z_m$ are as follows:

$$r_m'' + \frac{\gamma'}{\beta^2\gamma} r_m' = F_{rf} + F_{sc} \tag{21}$$

and

$$z_m'' + \left(\frac{2}{\beta^2\gamma^3} + \frac{1}{\gamma} \right) \gamma' z_m' = \frac{2k_z \alpha_{acc}}{\beta^2\gamma^3} \frac{dF}{dz} \sin(\Phi + k_z z) z_m - \frac{Q_b c}{I_A \beta^2 \gamma^4} \frac{1}{r_m z_m} \ , \tag{22}$$

where

$$F_{rf} = \frac{k_z \alpha_{acc}}{\beta^2\gamma} \left(-\frac{dF}{dz} \sin(\Phi + k_z z) + \beta\kappa F \cos(\Phi + k_z z) \right) r_m \tag{23}$$

and

$$F_{sc} = \frac{3}{2} \frac{Q_b c}{I_A \beta^2 \gamma^3} \frac{1}{r_m z_m} \left(1 - \frac{r_m}{3\gamma z_m} \right), \tag{24}$$

where F_{sc} is the space charge force, F_{rf} is focusing and defocusing RF force along the axis, I_A = 17000 A, and Q_b is the bunch charge.

The motion equations (19) and (20), and the coupled envelope equations (21) and (22) have been solved for the following initial variables: γ_0 = 1.01, initial phase $\Phi_0 = 40^0$ which is about optimum, $r_{m0} = 0.4mm$ corresponding to a UV laser spot size at the RF gun cathode, bunch length $2z_{m0} = 0.3mm$ corresponding to the 1 ps UV laser pulse duration. We use the bunch charge Q_b = 0.1 nC and the accelerating parameter a_{acc} = 0.82 corresponding to $E_{cathode}$ = 300 MV/m in these calculations. The results of the simulations are in good agreement with the MAGIC simulations using similar initial parameters (Fig. 10**).** It is also seen (Fig. 11) that the F_{sc} and F_{rf} are of similar magnitudes for the 0.1 nC case. This is consistent with the discrepancy between the single particle simulations and those including space charge.

3 DESIGN OF THE EXPERIMENT

The major system components of the MIT experiment are shown in Fig. 12. The RF gun cavity is located in a large vacuum vessel shown at the bottom of the diagram. The RF gun cavity is a traditional Brookhaven (BNL) style sidewall coupled 1.5 cell structure [23]. The RF gun is composed of three pieces of OFHC copper which are clamped together and attached as a single piece to the WR-62 coupling waveguide.

The experiment utilizes a 17 GHz relativistic klystron amplifier constructed by Haimson Research Corporation [24] to provide a 50 ns to 1 μs pulse of up to 26 MW of microwave power. The klystron is driven by a 580 kV, 1 μs flattop modulator pulse. A 0.27 μperv Thomson CSF gun produces a 120 A space-charge limited electron beam at 580 kV. The amplifier chain includes a TWTA to provide up to 5 W to the klystron. The klystron gain is approximately 60 dB.

The klystron amplifier has been found to generate power in spurious modes when connected to a mismatched load. Microwaves associated with these modes are slightly higher in frequency than the operating frequency of the klystron. To eliminate these modes, which reduce the stability and gain of the amplifier, a Bragg filter was designed and installed on the RF gun coupling waveguide. The Bragg filter structure is shown in Fig. 13. This filter is reflective for frequencies between 16.7 and 17.2 GHz, and transmits for higher frequencies. The use of the Bragg filter allowed cavity coupling at 17.15 GHz, while minimizing impedance mismatches at higher frequencies that would cause the spurious oscillations to occur. The power reflectivity, R^2, of the Bragg filter was found to be about 0.43 at 17.15 GHz through cold tests. While this is not optimal, it is sufficient for coupling breakdown threshold power levels into the RF Gun. Up to 8 MW of klystron power was coupled into the cavity, with amplitude stability of ±5%. Breakdown in the RF gun occurring on some shots with incident power exceeding 5 MW, however, usually limited operation to a lower incident power. Phase stability was also measured using a phase discriminator. Phase variation was found to be less than 8° from shot-to-shot and less than 4° during a single shot. Dark current of 0.5 mA was observed in the RF gun when 7.5 MW of microwave power was incident on the RF gun cavity [1]. This corresponds to a peak electric field of about 450 MV/m at the cathode for a 50 ns pulse.

One of the advantages of going to higher frequency is that for a given field gradient, G, the temperature rise of the RF gun inner surface due to the power dissipated on the walls decreases (i.e. $\Delta T \propto \omega^{-1/4} G^2$) [25,26]. This is despite an increase in the power dissipated per unit area ($dP/dS \propto \omega^{1/2} G^2$) thanks to the decrease in the filling time of the structure ($t_{Fill} \propto \omega^{-3/2}$) and corresponding decrease in the RF pulse length. Using the constant surface flux solution to the heat transfer equation [27], the maximum surface temperature rise for an incident pulse of length t_p is given by

$$\Delta T = \frac{2 q_s \sqrt{\alpha t_p / \pi}}{k} , \qquad (25)$$

where q_s is the power per unit area incident on the copper surface, α is the thermal diffusivity, and k is the thermal conductivity. This can be shown to be consistent with the aforementioned frequency scaling law. For a typical shot (i.e. 50 ns long, 5 MW incident power or 4 MW dissipated on the cavity walls) this yields a maximum temperature rise on the RF gun walls of about 80° C. However, the RF gun has also survived incident powers up to 8 MW, corresponding to a maximum temperature rise of about 130° C, which is encouraging for future prospects of higher power operation.

The laser beam for the RF gun photocathode is generated by a Ti:Sapphire laser system, which produces 2 ps, 1.5 mJ, 2 mm diameter pulses at 780 nm after chirped pulse amplification. The pulse duration of 2 ps was verified using a single-shot autocorrelator. Pulse-to-pulse laser energy fluctuations are approximately ±10%. These pulses are frequency tripled to 10-20 μJ of UV, and then focused on the back wall of the copper cavity. The ultraviolet spot size is approximately 1 mm in diameter. A UV pulse length of 1 ps is estimated from the measured infrared 2 ps pulse duration using nonlinear optical theory. Measurement of the frequency sidebands using a spectrum analyzer [28] indicated a laser phase jitter of less than 5 ps, or 30 degrees.

The timing scheme used in the MIT RF gun experiment is slightly different from that of other photocathode experiments. A photodiode samples the light pulses bouncing back and forth in the optical cavity of the Ti:Sapphire laser oscillator. The IR pulses of this oscillator are used as input to a regenerative amplifier. The frequency of these pulses is 84 MHz and is dictated only by the length of the cavity. No external oscillator is used. The signal from this photodiode is used as input to a frequency multiplier box, which filters and amplifies the signal. The output signal is about 17.15 GHz and is phaselocked to the laser system. This milliwatt level signal is used as input to the microwave amplifier chain which drives the RF gun experiment. Phase stability of this system has been verified by measuring the percentage of shots resulting in successful electron beam production vs. injection phase of the laser pulse into the RF Gun (Fig. 14). Theoretically, emission should be observed over about 100 degrees of injection phase (see Fig. 8). The

observed width of the experimental curve is consistent with a combined laser and microwave source phase jitter of better than ± 20°.

4 EXPERIMENTAL RESULTS

An example of a typical cavity filling shot is shown in Fig. 15. The forward and reflected power are measured at the directional couplers immediately before the RF Gun (see Fig. 12). The stored energy in the cavity (and hence the accelerating gradient) in the absence of beam loading can be calculated from a modified power conservation equation,

$$\frac{dW}{dt} = k_{Br}^2 P_{inc} - P_{refl} - \frac{\omega}{Q_{cav}} W \,, \tag{26}$$

where W is the stored energy in the cavity, Q_{cav} is the unloaded quality factor, and k_{Br} is a factor that accounts for the reflectivity R of the Bragg filter and can be derived from equations (13) and (14) to give

$$k_{Br}^2 = \left(\frac{R - \frac{1+R}{2}\beta_c}{1 + \frac{1+R}{2}\beta_c} \right)^2 + \frac{(1+R)^2 \beta_c}{\left(1 + \frac{1+R}{2}\beta_c\right)^2} = 0.90 \,, \tag{27}$$

for R = 0.67 and β = 1.56. These measurements demonstrate that peak accelerating fields of over 300 MV/m have been achieved at the cathode for incident power levels exceeding 4 MW. This corresponds to an average accelerating gradient of about 200 MV/m over the half cell and about 80 MV/m over both the half and full cells combined.

The beam diagnostics so far employed in this experiment consist of a high speed Faraday cup for beam bunch charge measurements and a Browne and Buechner style magnetic spectrometer [29] for beam energy and energy spread measurements. The Faraday cup is designed as a conical tapered 50 Ω transmission line. The central conductor is 1 cm in

diameter with a 5 mm diameter center collector. The laser beam is injected into the RF gun with the use of a prism placed in the collector portion of the Faraday cup (Fig. 16). During early experiments, it was discovered that rectified microwave signals were dominating the detected Faraday cup signals. In order to eliminate this effect, it was necessary to place a 5 mm radius cylindrical collimator between the RF gun and the Faraday cup to act as a cutoff waveguide. Integrated Faraday cup signals indicated a total bunch charge of up to 0.1 nC (Fig. 17-a).

Multiple pulse generation by sequential laser pulses has also been observed with this experimental set up. As many as three separate laser pulses can be produced through imperfect dumping of the regenerative amplifier cavity. These laser pulses are separated in time by the round trip time of the cavity (about 9 ns), which is close enough to an integer multiple of RF periods (about 155) to result in up to three corresponding electron beams (Fig. 17-b). The laser pulses seen in Fig. 17 are detected by picking off a small portion of the laser pulse immediately before injection into the RF Gun and detecting it with a photodiode. In the future, we plan to employ optical beam splitters to intentionally produce a train of optical pulses and a corresponding train of electron beam bunches.

The magnetic spectrometer used to perform the measurement of the beam energy is a circular magnetic field boundary, field radius $R = 10\ cm$, 1 cm gap size, 1 kilo-Gauss saturation structure. The beam is bent approximately 90° and detected by detectors placed on the focal plane of the spectrometer. The determination of the detector placement (i.e. the location where a monochromatic divergent beam from a point source is geometrically focused back to a point) in a basic Browne-Buechner spectrometer design is determined by the ratio of the field radius R to the distance L between the electron source and the magnetic field boundary. The equation for the focal plane assuming the coordinate system shown in Fig. 18 is

$$\tilde{y} = \frac{\left(2\tilde{L}+1\right)}{\tilde{L}^2}\tilde{x}^2 - 2\left(\frac{1+\tilde{L}}{\tilde{L}}\right)^2 \tilde{x} + \left(\frac{1+\tilde{L}}{\tilde{L}}\right)^2, \qquad (28)$$

where $\tilde{L} = L/R$, $\tilde{x} = x/R$, and $\tilde{y} = y/R$, and can be derived using the same procedure as in the original Browne-Buechner paper [29], but without assuming $R=L$. The effect of increasing L relative to R is to move the focal plane closer to the magnetic field boundary and to decrease the slope. Ideally, one would like to avoid doing this since the dispersion on the focal plane will accordingly decrease. For our measurement, the electron source was taken to be the RF Gun exit. This simplified the beam line design by eliminating the need for a pinhole or focusing elements. The size of the RF gun housing structure and the necessity of the collimator limited the minimum drift length between the RF Gun exit and the magnetic field boundary of the spectrometer to $L = 30$ *cm*, or $\tilde{L} = 3$ (Fig. 18). Simulations of the energy measurement using PARMELA [30] indicate that after traversing the distance between the RF gun and the spectrometer, the rms energy spread of a 1 MeV beam is about 2.2 %. The increase from the rms energy spread of about 1.5% at the exit of the gun is due to longitudinal space charge forces.

Two types of energy measurements were performed with this setup. The first utilized a single Faraday cup placed on a 90° arc from the beam line. The percent energy acceptance of this detector was about 10%. The low energy end of the detector was approximately located at the focal plane of the spectrometer, allowing for an accurate measurement of the maximum energy of the beam by observing the maximum magnetic field for which a beam is detected over many shots. These measurements yielded electron energies as high as 1.1 MeV. The second type of energy measurement utilized an array of up to six detectors, consisting of 2mm wide Faraday cups placed side by side along the focal plane (Fig. 18). Due to mechanical constraints, the array was placed on the low energy, low dispersion end of the focal plane, resulting in a maximum energy resolution of about 2.2%. This measurement provided similar results as the other measurement, yielding energies up to 1.1 MeV and single shot rms energy spreads as small as ± 2.5% (Fig. 19), roughly in accordance with simulations.

Both energy measurements yielded results that are consistent with simulations in terms of the energy of the beam, indicating maximum accelerating gradients of over 300 MV/m at the cathode (200 MV/m average over the first cell) consistent with the theoretical analysis in section 2 and the measurement of the stored energy shown in Fig. 15. The 2

to 3 % measured rms energy spread at the spectrometer is also roughly in accordance with theoretical expectations. From PARMELA simulations of space charge effects during transport of the beam, these results are consistent with an energy spread of about 1.5 % at the exit of the RF gun.

5 CONCLUSIONS AND FUTURE PLANS

The experimental results presented here for the MIT 17 GHz RF Gun demonstrate the potential for high gradient acceleration at high microwave frequencies. Measurements of the electron beam energy as well as high power measurements of the cavity filling of the gun suggest peak accelerating fields of about 0.3 GV/m. These measurements are consistent with theoretical studies of the RF Gun coupling and beam dynamics also presented here. Up to three separate electron bunches have been produced on a single shot corresponding to the splitting of the laser pulse. Analysis of the temperature rise of the RF gun walls indicate peak temperature rises of about 80° C corresponding to peak on axis electric fields of about 300 MV/m were sustained without damage to the RF gun. In order to demonstrate the superior beam quality promised by high frequency, high gradient RF Guns, plans for measuring the emittance of the electron beam as well as plans for the development of an improved, better field balanced cavity are underway. Eventually, an emittance compensated gun will be employed with the hope that a record high brightness electron beam will be produced.

AKNOWLEDGEMENTS

This work is supported by D.O.E. H.E.P contract number DE-FG02-91ER40648. We would also like to thank Dr. Jake Haimson and Haimson Research Corporation for use of the klystron amplifier, as well as Ivan Mastovsky and Bill Mulligan, whose dedication and expertise have been instrumental in the operation of this experiment.

REFERENCES

[1] S. Trotz, W.J. Brown, B.G. Danly, J.P. Hogge, M. Khusid, K.E. Kreishcer, M. Shapiro, R.J. Temkin, "High Power Operation of a 17 GHz Photocathode RF Gun," Advanced Accelerator Concepts, Seventh Workshop, S. Chattopadhyay, J. McCullough, P. Dahl, editors, AIP Conf. Proc. 398, AIP Press, Woodbury, NY, pp. 717-729 (1996).

[2] D.T. Palmer, X.J. Wang, I. Ben-Zvi, R.H. Miller, "Beam Dynamics Enhancement due to Accelerating Field Symmetrization in the BNL/SLAC/UCLA 1.6 cell S-Band Photocathode RF Gun," to be published in Proceedings of the 1997 Particle Accelerator Conference, IEEE Press (1997).

[3] D.T. Palmer, X.J. Wang, R.H. Miller, M. Babzien, I. Ben-Zvi, C. Pellegrini, J. Sheehan, J. Skaritka, H. Winick, M. Woodle, V. Yakimenko, "Emittance Studies of the BNL/SLAC/UCLA 1.6 cell Photocathode rf Gun," to be published in Proceedings of the 1997 Particle Accelerator Conference, IEEE Press (1997).

[4] K. Aulenbacher, R. Bossart, H. Braun, J. Clendenin, J.P. Delahaye, J. Madsen, G. Mulhollan, J. Sheppard, G. Suberlucq, and H. Tang, "Initial Test of an RF Gun with a GaAs Cathode Installed," Stanford Linear Accelerator Laboratory Publication, SLAC-PUB-7299 (1996).

[5] S.C. Hartman, N. Barov, C. Pellegrini, S. Park, J. Rosenzweig, G. Travish, R. Zhang, C. Clayton, P. Davis, M. Everett, C. Joshi, G. Hairapetian, "Initial measurements of the UCLA rf photoinjector," Nucl. Instr. and Meth. A 340, pp. 219-230 (1994).

[6] R. Bossart, H. Braun, M. Dehler, J.C. Godot, "A 3 GHz photoelectron gun for high beam intensity," Nucl. Instr. and Meth. A 375, ABS 7-8 (1996).

[7] Y.C. Huang, R.H. Pantell, J.F. Schmerge, J.W. Lewellen, J. Feinstein, "Electron Beam Characterization for a Compact Far-Infrared Free-Electron Laser," IEEE Journal of Quantum Electronics, Vol. 31, No. 9, pp. 1637-1641 (1995).

[8] M.H. Woodle, K. Batchelor, J. Sheehan, "Mechanical Design of a RF Electron Gun," 1988 Linear Accelerator Conference Proceedings, pp. 351-2 (1989).

[9] D.W. Feldman, et. al., "Experimental Results from the Los Alamos FEL Photoinjector", IEEE Journal of Quantum Electronics, Vol. 27, No. 12., pp. 2636-2643 (1991).

[10] R.L. Sheffield, E.R. Gray, J.S. Fraser, "The Los Alamos Photoinjector Program," Nucl. Instr. and Meth. A 272, pp. 222-226 (1988).

[11] LeSage, G.P., "A High Brightness, X-Band Photoinjector for the Production of Coherent Synchrotron Radiation," Bull. Am. Phys. Soc., Vol. 42, No. 10, pp. 1837-8 (1997).

[12] Kwang-Je Kim, "RF and Space-Charge Effects in Laser-Driven RF Electron Guns," Nucl. Instr. and Meth. A 275, pp. 201-218 (1989).

[13] L. Serafini, "Analytical Description of Particle Motion in Radio-Frequency Photo-Injectors," Particle Accelerators, Vol. 49, pp. 253-271 (1995).

[14] L. Serafini, J. Rosenzweig, "Envelope analysis of intense relativistic quasilaminar beams in rf photoinjectors: A theory of emittance compensation," Physical Review E, Vol. 55, No. 6, pp. 7565-7590 (1997).

[15] J. Rosenzweig, E. Colby, "Charge and Wavelength Scaling of RF Photoinjector Designs," Advanced Accelerator Concepts, P. Schoessow, editor, AIP Conf. Proc. 335, AIP Press, Woodbury, NY pp. 724-737 (1995).

[16] Leon C.-L. Lin, S.C. Chen, J.S. Wurtele, “On the frequency scaling of electron guns,” Advanced Accelerator Concepts, P. Schoessow, editor, AIP Conf. Proc. 335, AIP Press, Woodbury, NY, p. 704 (1995).

[17] Leon C.-L. Lin, S.C. Chen, J.S. Wurtele, “An equivalent network analysis of waveguide broad-wall coupled RF gun structures,” Nucl. Instr. and Meth. A 275, pp. 274-284 (1997).

[18] T. Weiland. “On the computation of resonant modes in cylindrically symmetric cavities”, Nucl. Instr. and Meth., Vol. 216, No.3, pp. 329-48, (1983).

[19] R.E. Collin, “Field Theory of Guided Waves,” IEEE Press (1991).

[20] B. Radak, R.L. Gluckstern, “Penetration of electromagnetic fields through an elliptical hole in a wall of finite thickness,” IEEE Trans. Microwave Theory Tech., Vol. 43, No.1, pp. 194-204 (1995).

[21] Bruce Goplen et. al. MAGIC User’s Manual, 1991. Mission Research Corporation Technical Report MRC/WDC-R246.

[22] M.Reiser, “Theory and Design of Charged Particle Beams,” John Wiley & Sons, Inc. (1994).

[23] K. T. McDonald, “Design of the Laser-Driven RF Electron Gun for the BNL Accelerator Test Facility,” IEEE Transactions on Electron Devices, Vol. 35, No. 11, pp. 2052-2059 (1988).

[24] J. Haimson and B. Mecklenburg, "Initial Performance of a High Gain, High Efficiency 17 GHz Traveling Wave Relativistic Klystron for High Gradient Accelerator Research," Pulsed RF Sources For Linear Collider, Richard C. Fernow, editor, AIP Conf. Proc. 337, AIP Press, Woodbury, NY, pp. 146-159 (1995).

[25] P. Wilson, "Scaling Linear Colliders to 5 TeV and Above," Stanford Linear Accelerator Laboratory publication, SLAC-PUB-7449, (1997).

[26] D. Whittum, H. Henke, and P.J. Chou, "High-Gradient Cavity Beat-Wave Accelerator at W-Band," to be published in Proceedings of the 1997 Particle Accelerator Conference, IEEE Press, (1997).

[27] F. Incropera and D. Dewitt, "Introduction to Heat Transfer," Second Edition, John Wiley & Sons, NY, p.260 (1990).

[28] D. von de Linde, "Characterization of the noise in continuously operating mode-locked lasers," Appl. Phys. B, p. 201 (1986).

[29] C.P. Browne and W. W. Buechner, "Broad-Range Magnetic Spectrograph", The Review of Scientific Instruments, Vol. 27, No. 11, pp. 899-907 (1956).

[30] J.H. Billen, PARMELA User's Manual, Los Alamos Accelerator Code Group (LAACG), LA-UR-96-1835.

Parameter	Label	Value
Loaded Q	Q_L	1100
Unloaded Q	Q_{cav}	2700
Coupling Coefficient	β_c	1.56
Polarizabilities	α_1	$6.85*10^{-9}$ m^3
	α_2	$7.10*10^{-9}$ m^3

Table 1: Measured RF Gun Characteristics

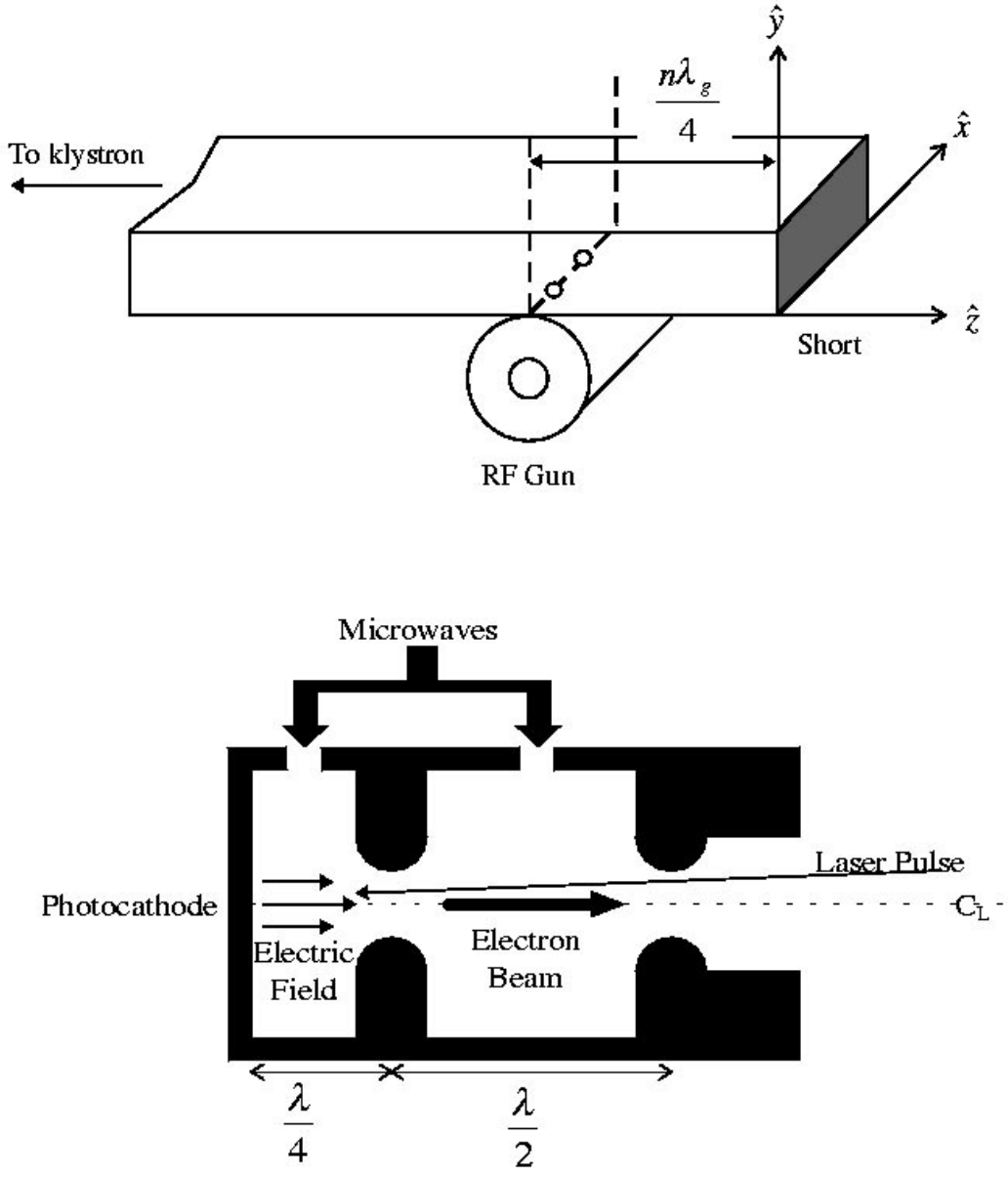

Figure 1: Cross section of RF gun (bottom) and illustration of RF coupling scheme (top).

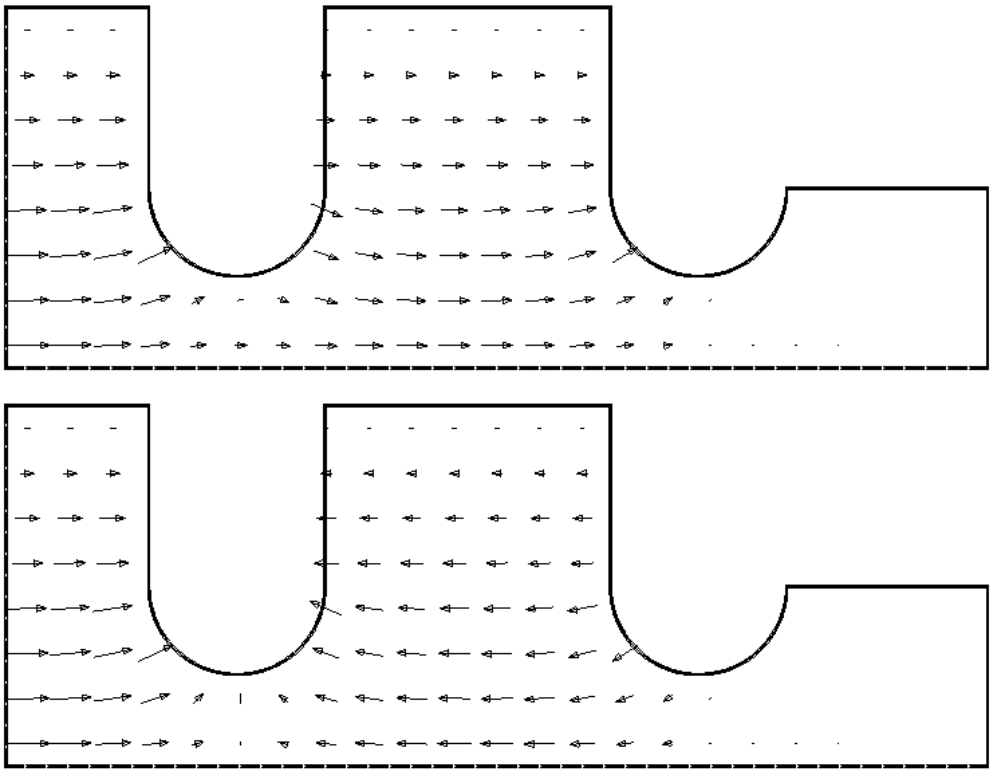

Figure 2: Normal modes of a 1 ½ cell RF gun (Top: 0-mode; Bottom: π-mode).

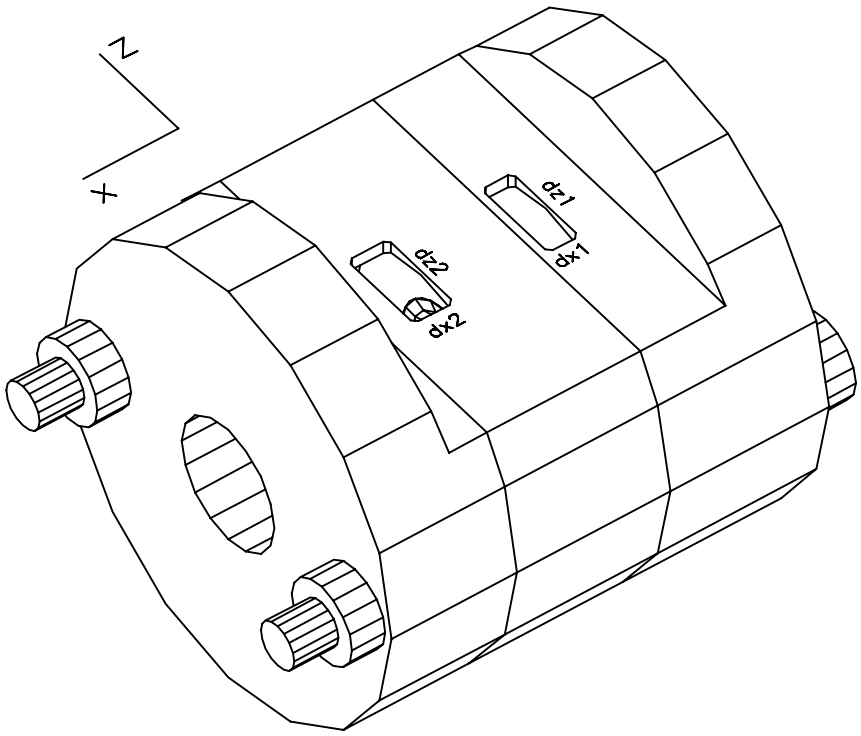

Figure 3: Close up of the RF gun with coupling holes.

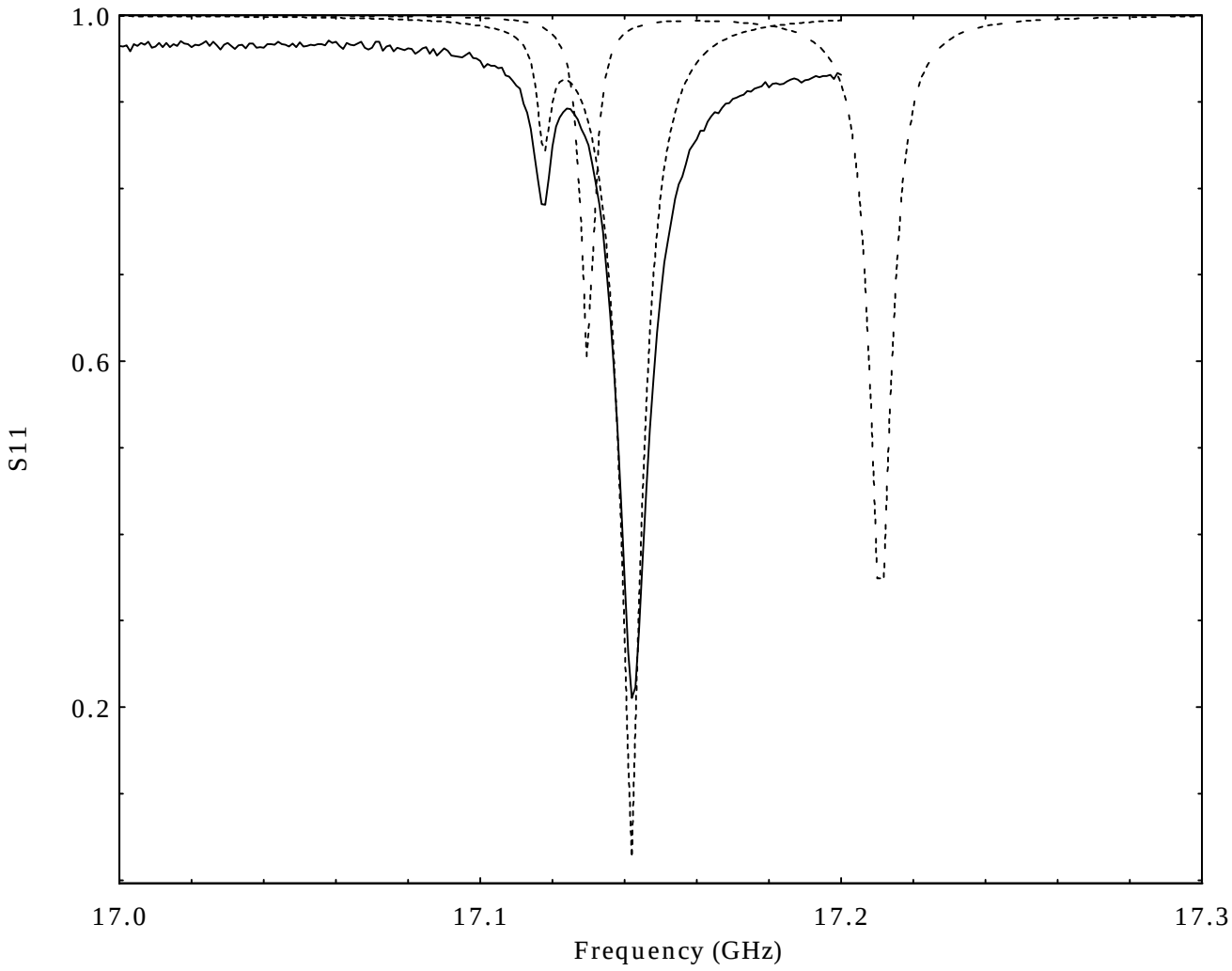

Figure 4: Comparison of experimental and theoretical S_{11} curves. Solid line: measured S_{11} curve. Dotted line: theory for matched polarizabilities. Broken dotted line: theory for directly calculated polarizabilities.

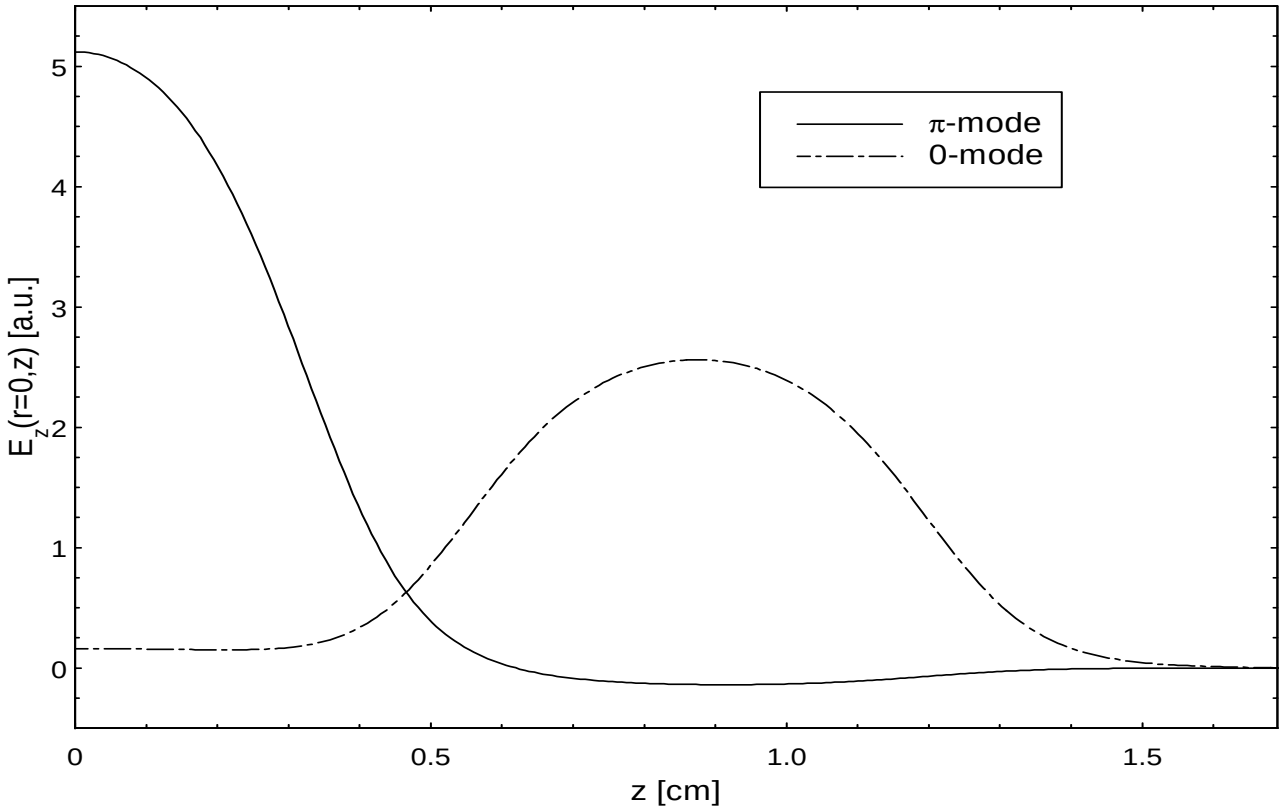

Figure 5: Eigenmodes of the RF gun calculated with SUPERFISH.

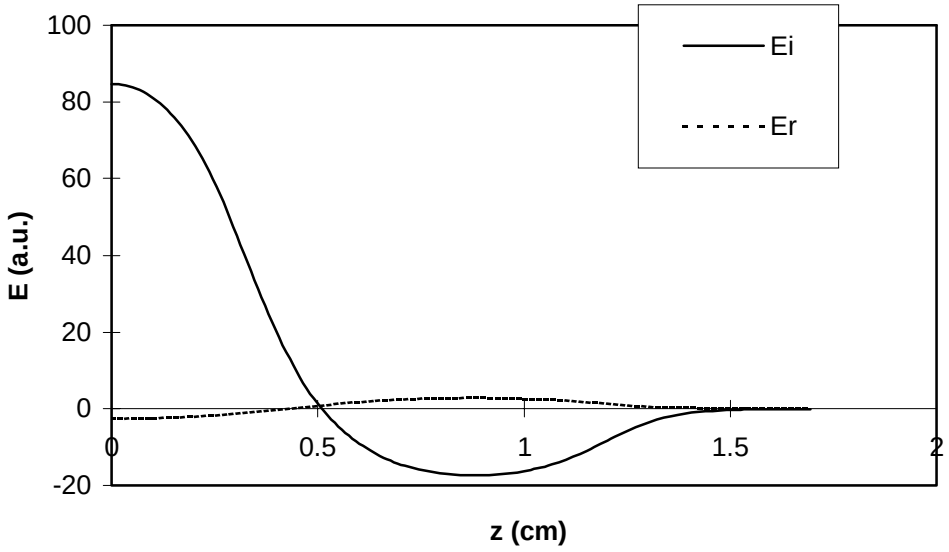

Figure 6: Actual on axis complex field profile of the RF gun calculated with coupling hole theory using the SUPERFISH eigenmodes.

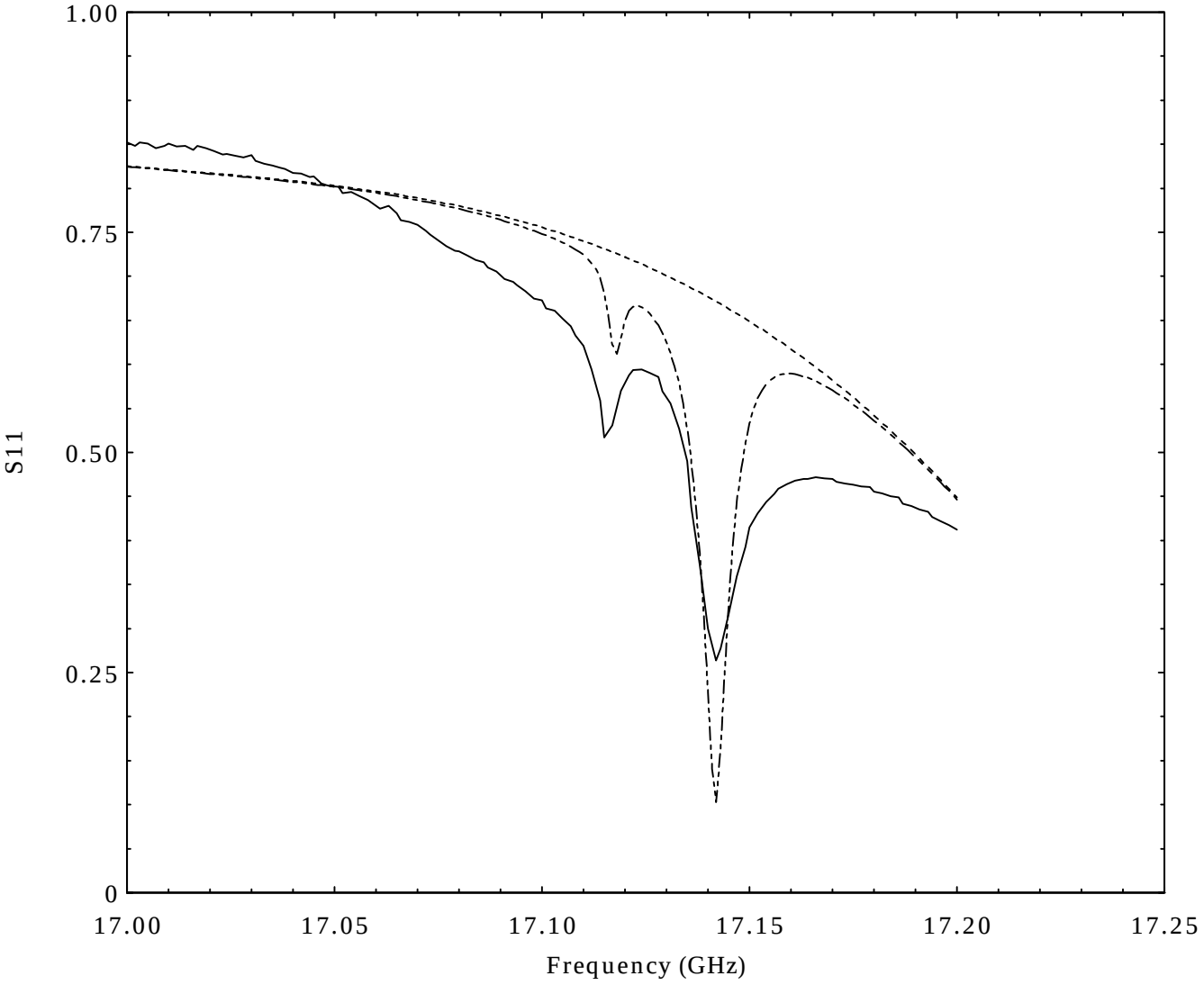

Figure 7: Measured and theoretical S_{11} curve with the Bragg Filter attached to the RF gun. Solid line: measured S_{11} curve of the RF gun. Broken dotted line: theoretical S_{11} curve. Dotted line: measured reflectivity of the Bragg filter.

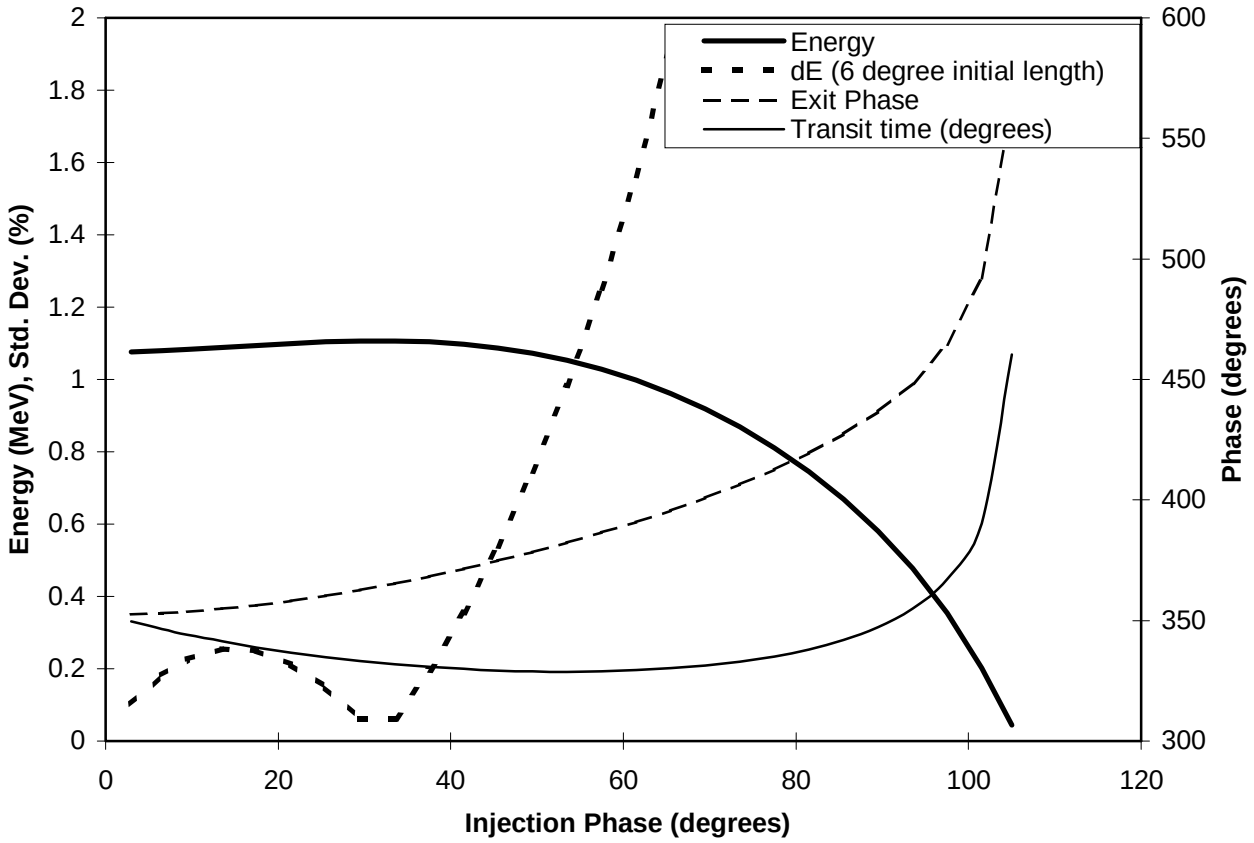

Figure 8: Single particle simulation results. The peak field at the cathode is 300 MV/m.

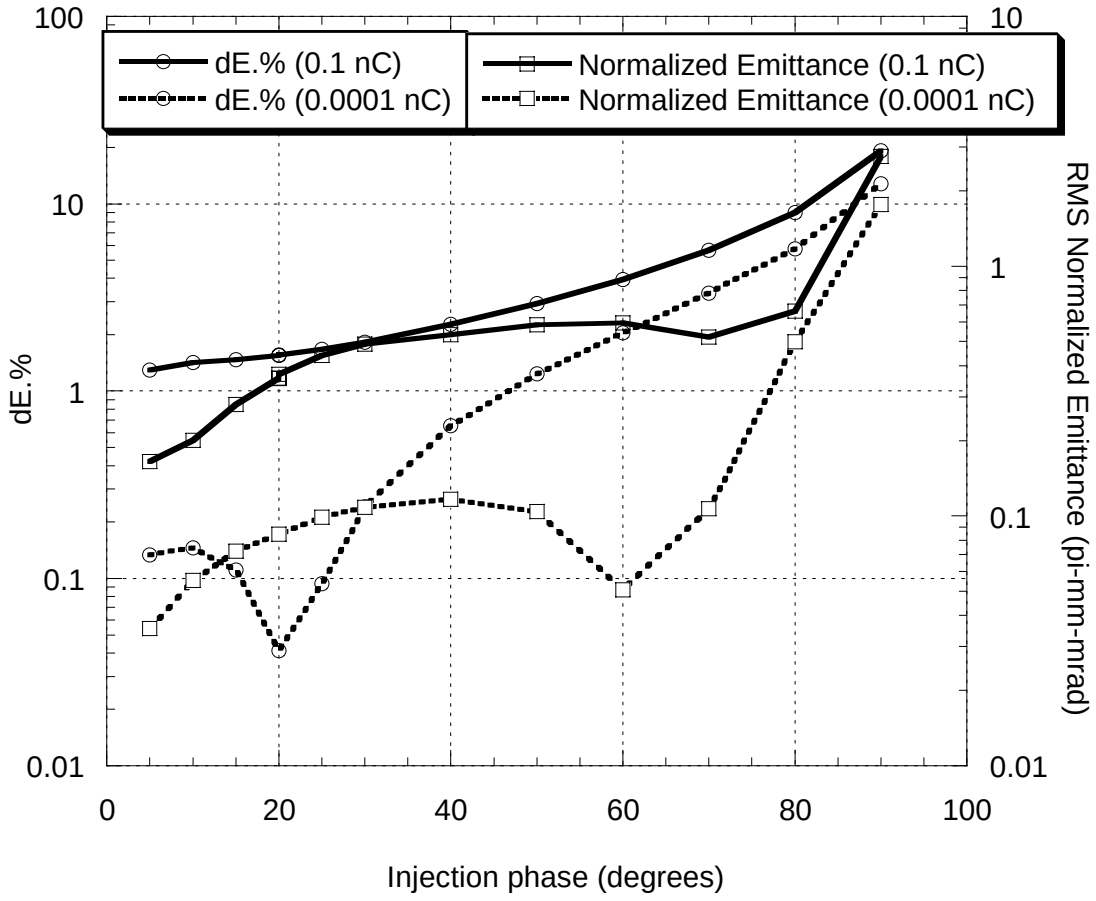

Figure 9: Comparison of Magic simulations with high (0.1 nC) and low (0.0001 nC) space charge. The circles correspond to rms energy spread (left axis) while the squares correspond to rms normalized emittance (right axis). The maximum on axis electric field at the cathode is 300 MV/m while the initial beam length and radius are 1 ps and 0.4 mm respectively.

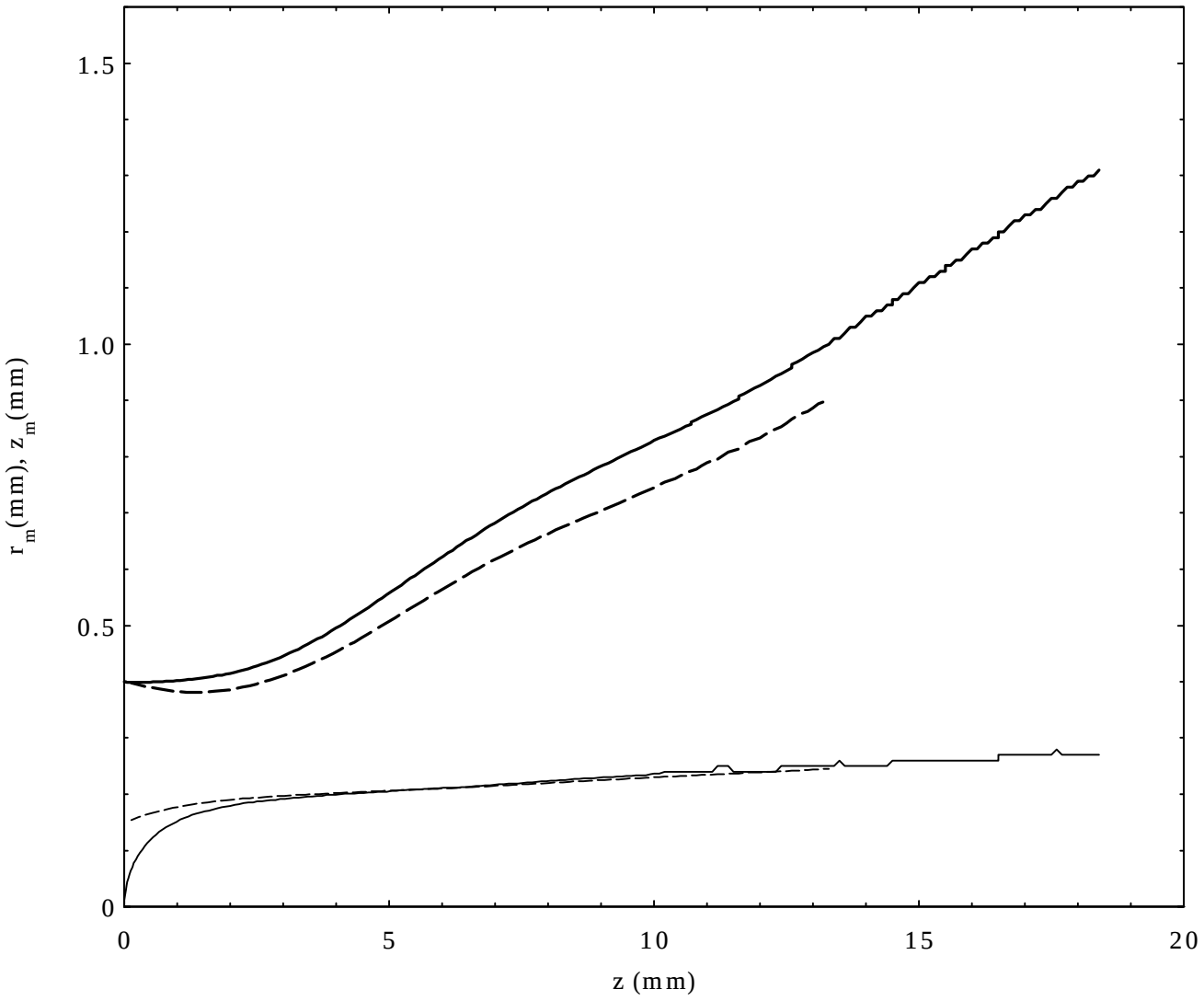

Figure 10: Comparison of MAGIC simulations (solid lines) and Envelope Equation Analysis (dotted lines) of the maximum radius (heavy lines) and length (thin lines) of an electron bunch while being accelerated in the RF gun with initial radius 0.4 mm, initial length 0.3 mm, and bunch charge 0.1 nC. The maximum electric field at the cathode (z=0) is taken to be 300 MV/m.

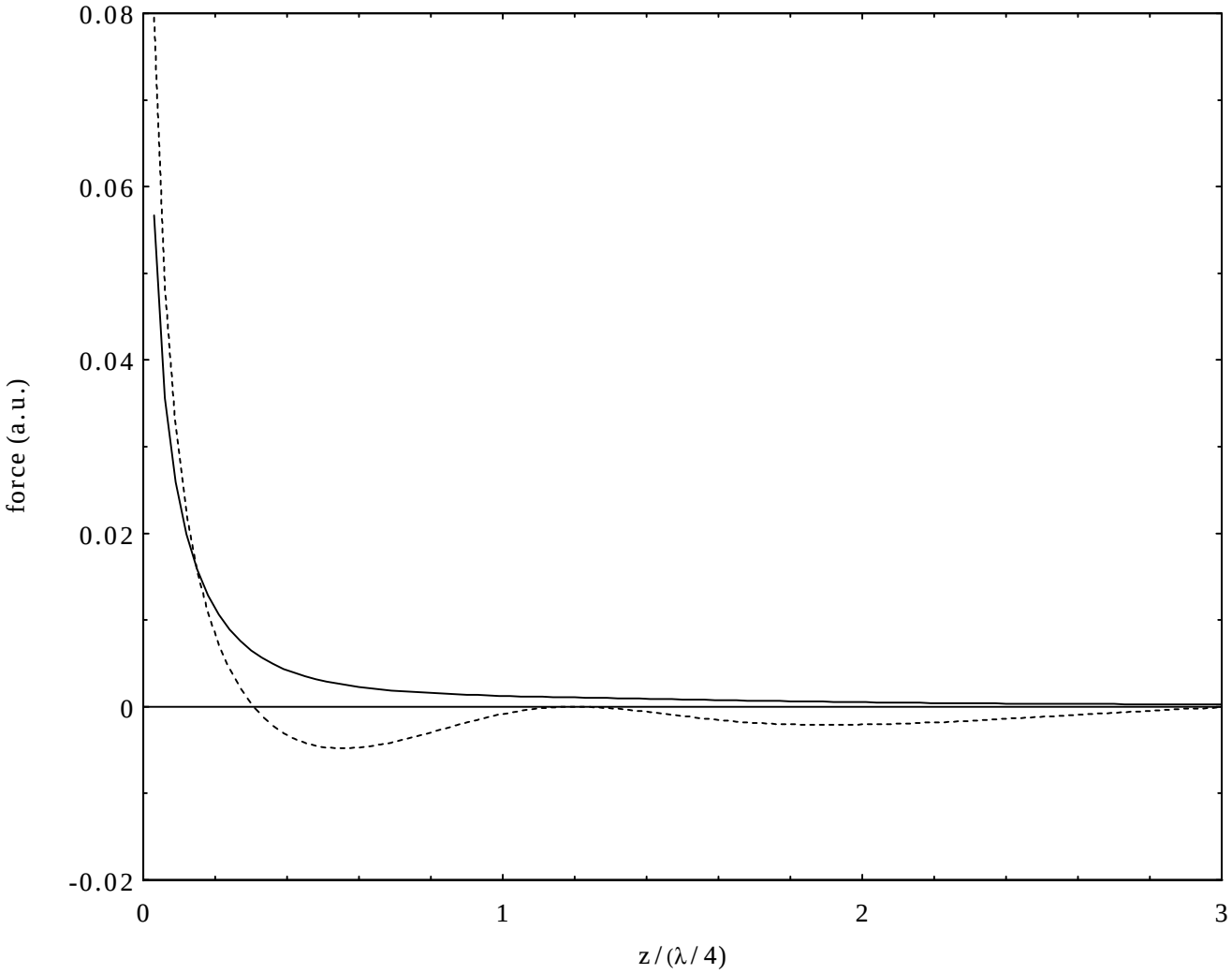

Figure 11: Comparison of space charge to RF forces in the RF gun.
Solid line: space charge force. Dotted line: RF force.

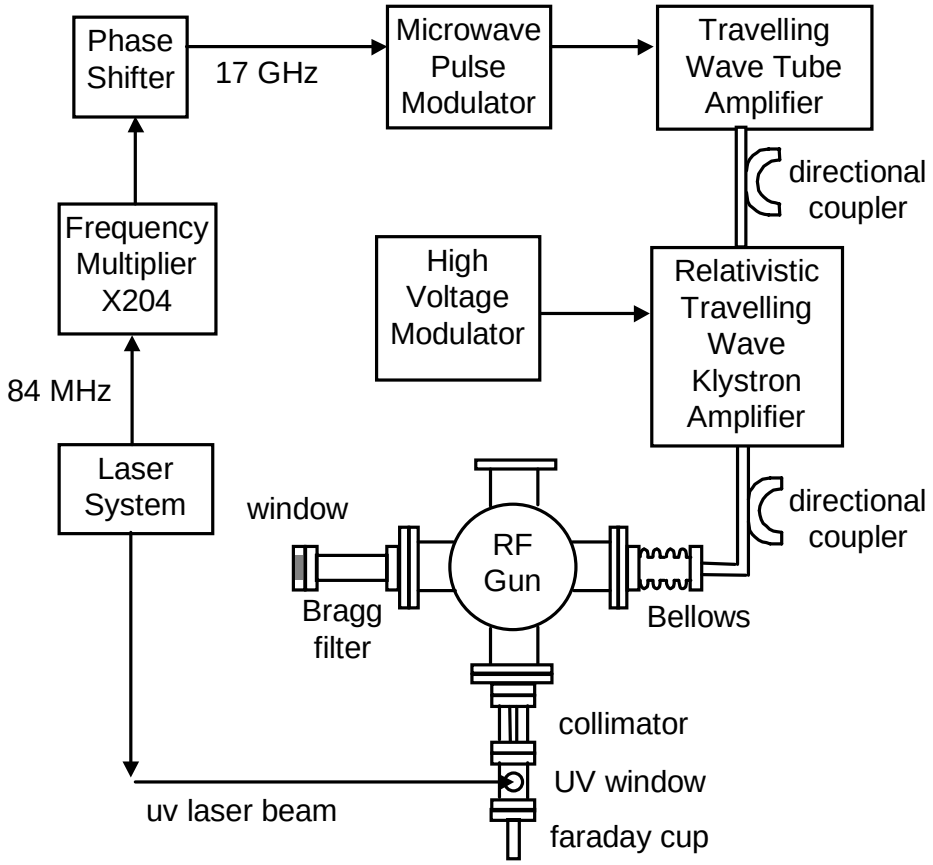

Figure 12: Schematic of the experiment (not to scale).

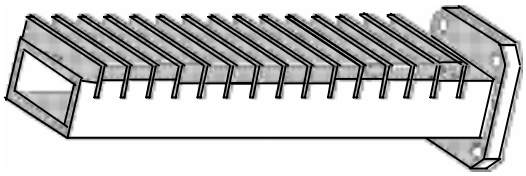

Figure 13: Illustration of the Bragg Filter.

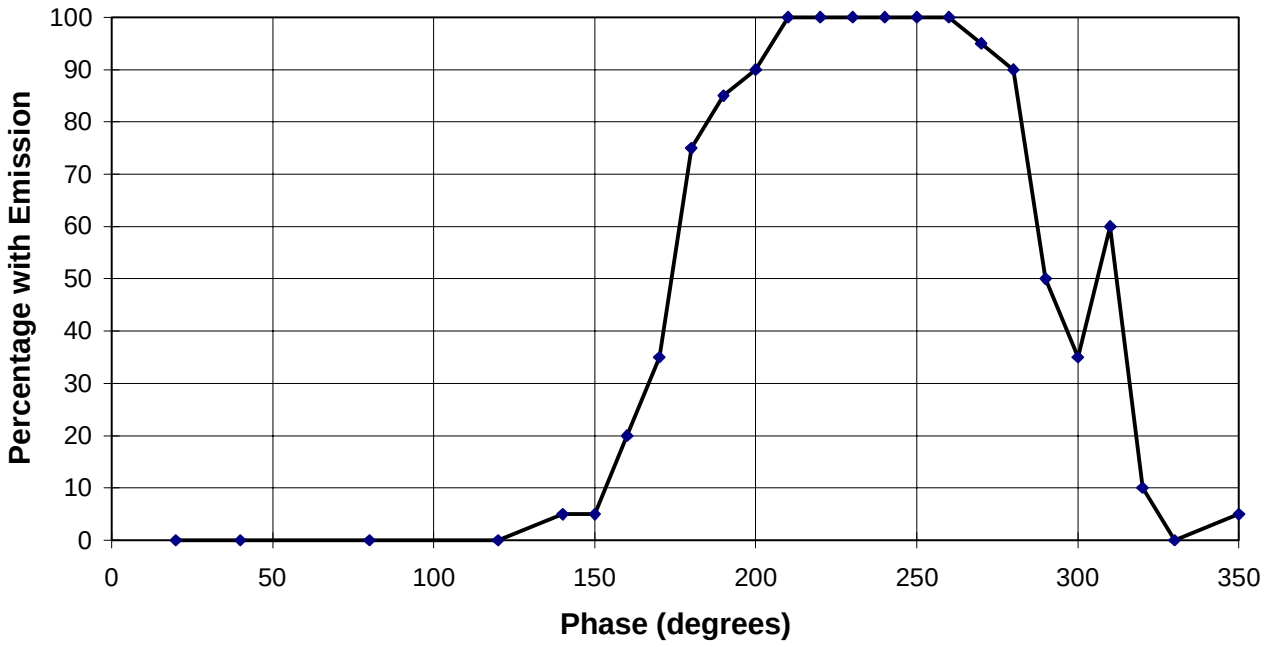

Figure 14: Laser to RF phase stability measurement.

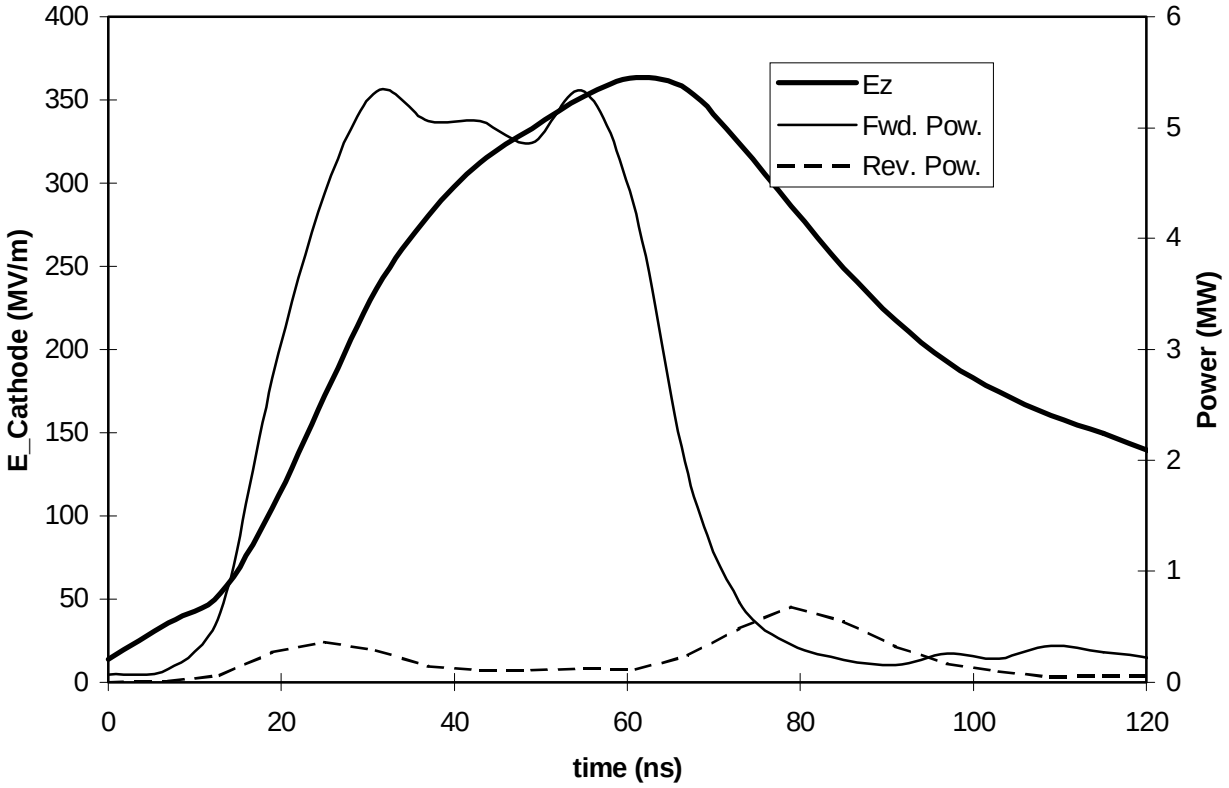

Figure15: Cavity filling measurement illustrating the peak field at the cathode.

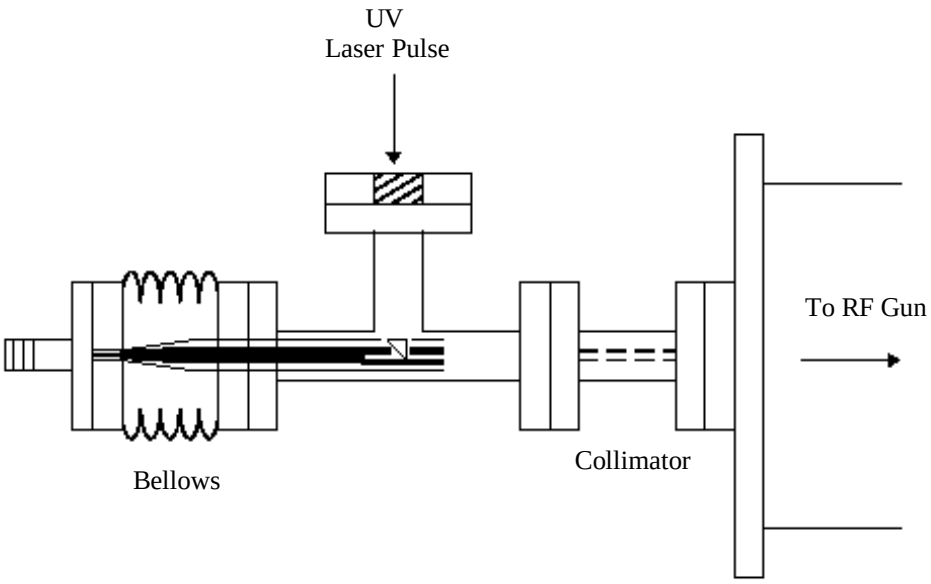

Figure 16: Faraday cup setup for bunch charge measurement.

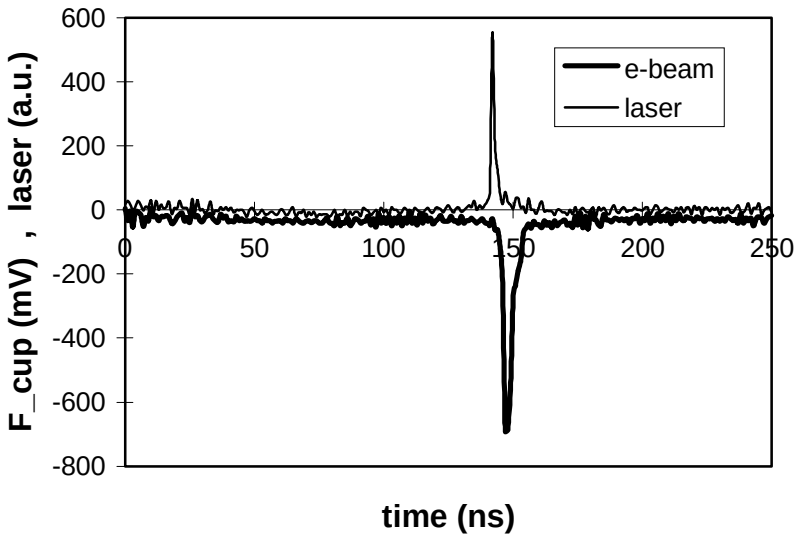

Figure 17-a: Laser induced electron beam emission from RF gun.

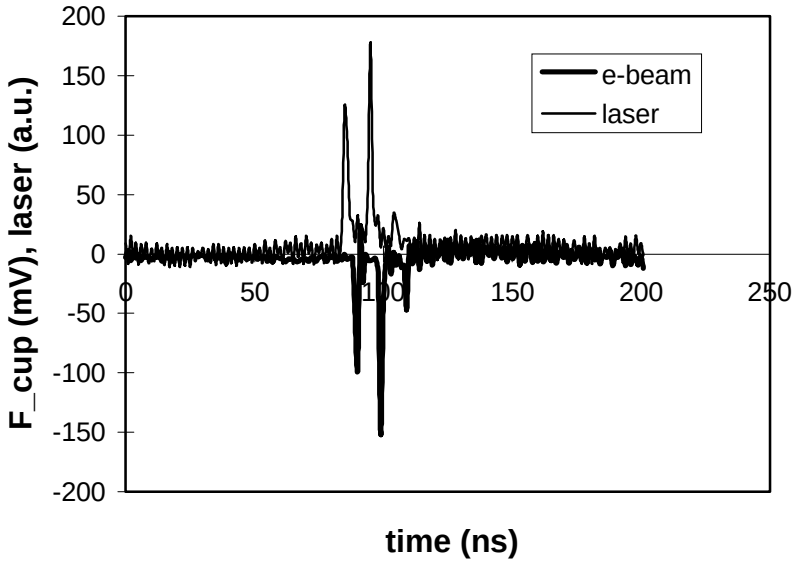

Figure17-b: An example of multiple electron bunch generation.

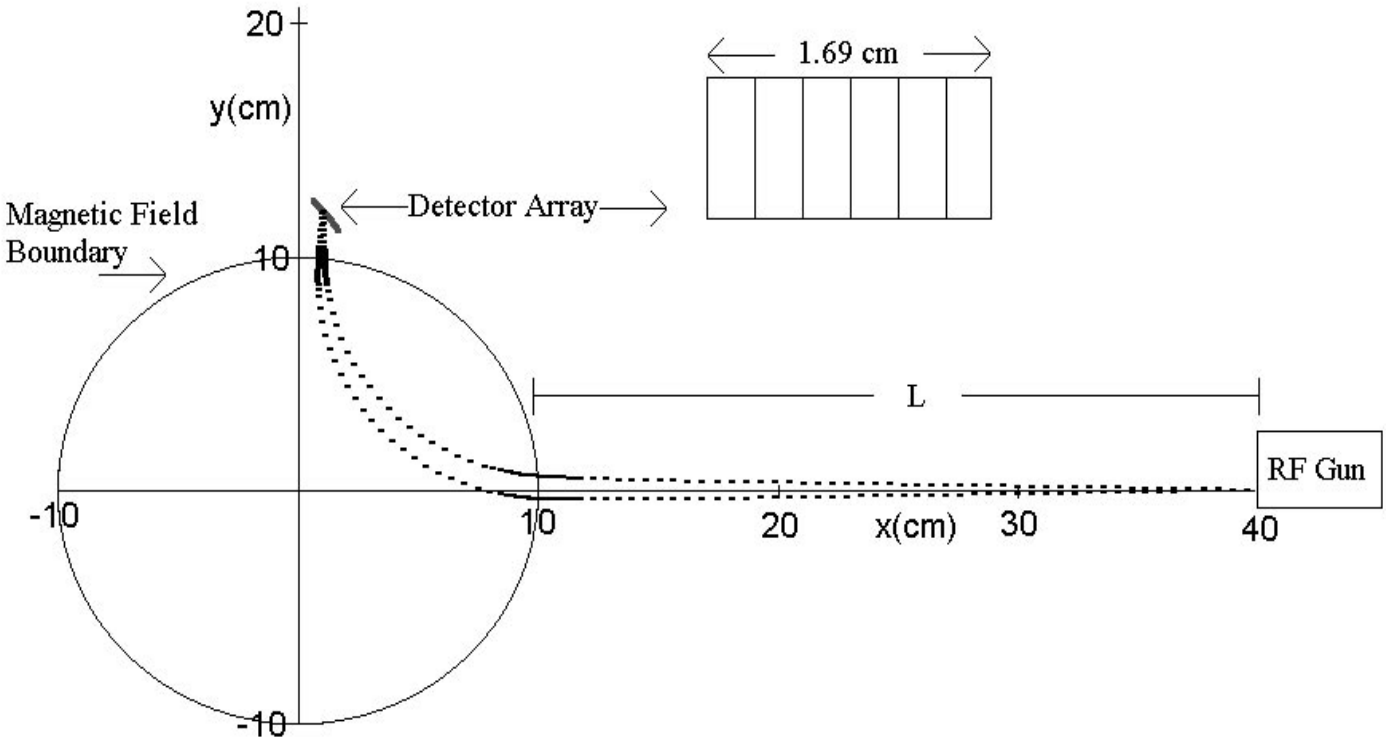

Figure 18: Illustration of the energy spread measurement.

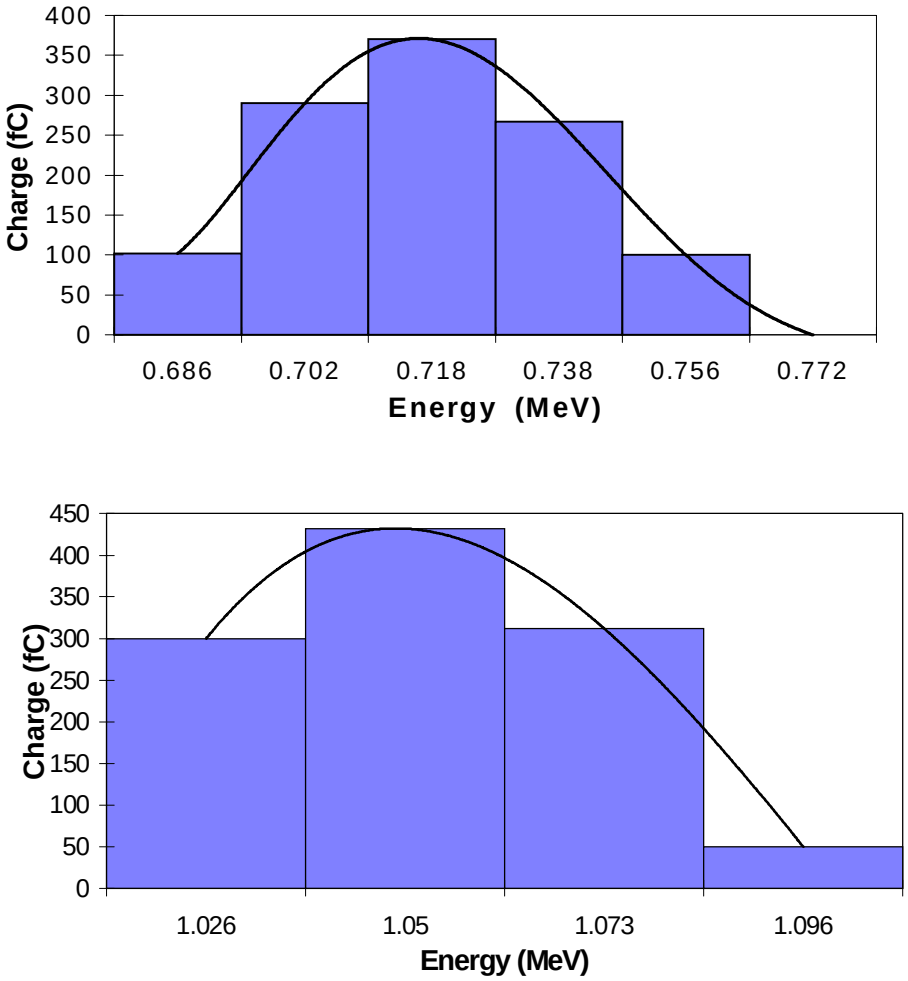

Figure 19: Measurements of Electron Beam Energy.